High Field Electrical Polarization and Magnetoelectric Coupling in Chiral Magnet [Cu(pym)(H₂O)₄]SiF₆·H₂O

Avery L. Blockmon,[⊥] Minseong Lee,[⊥] Shengzhi Zhang, Zachary E. Manson, Jamie L. Manson, Vivien S. Zapf, and Janice L. Musfeldt*

Read Online

ACCESS | 📊 Metrics & More | 📖 Article Recommendations | 🔲 Supporting Information

ABSTRACT: The Heisenberg antiferromagnetic chain is a canonical model for understanding many-body gaps that emerge in quantum magnets, and as a result, there has been significant work on this class of materials for much of the past century. Chiral chains, on the other hand, have received markedly less attention. $[Cu(pym)(H_2O)_4]SiF_6 \cdot H_2O$ (pym = pyrimidine) is an $S = 1/2$ chiral antiferromagnet with an unconventional spin gap and no long-range ordering at zero field, features that distinguish it from more conventional spin chains that host simple phase diagrams and no magnetoelectric coupling. Here, we report pulsed magnetic field electrical polarization measurements, strong magnetoelectric coupling, and extraordinary magnetic field - temperature phase

diagrams for this system. In addition to three low field transitions, we find a series of phase transitions between 40 and 70 T that depend on the magnetic field direction. The observation of electric polarization in a material with a nonpolar crystal structure implies symmetry-breaking magnetic ordering that creates a polar axis - a mechanism that we discuss in terms of significant interactions between the chiral chains as well as Dzyaloshinskii−Moriya effects. Further, we find second-order magnetoelectric coupling, allowing us to deduce the magnetic point group of the highest polarization phase. These findings are in contrast to expectations for an unordered one-dimensional spin chain and reveal a significantly greater complexity of behavior in applied field.
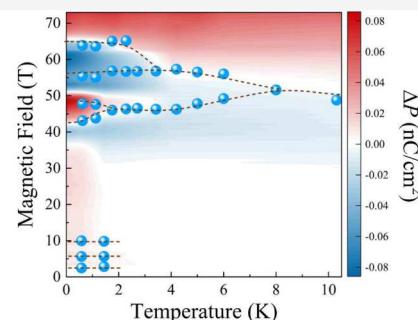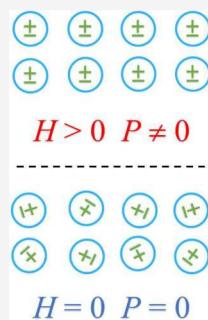
INTRODUCTION

Quantum spin chains are the fundamental building blocks of quantum magnetism. As we seek to understand magnets of increasing complexity, starting with a single spin and working our way up to many body systems, the linear spin chain is the first system we encounter that shows quantum many-body behavior in the form of gaps, collective excitations, fractionalized excitations, and order parameters.[1−4] Surprisingly, *chiral* spin chains are under-explored, despite the fact that chirality is implicated in a number of exciting and unexpected properties.[5−13] $[Cu(pym)(H_2O)_4]SiF_6 \cdot H_2O$ was recently recognized as a chiral spin chain with properties that differ significantly from those of a traditional linear spin chain.[14,15] This metal−organic material forms chiral chains of $S = 1/2$ Cu^{2+} ions along the c-axis where the spiral has a periodicity of four Cu centers [Figure 1(a)]. The Cu spins are interspersed by meta-linked pyrimidines that provide the primary exchange interaction along the chains.[3,14,15] The exchange interaction is antiferromagnetic ($J = -42$ K) based on susceptibility, heat capacity, and magnetization.[15] Even so, there is no long-range ordering above 20 mK at zero magnetic field.[15] The chirality of the crystal imposes itself on the magnetism via Dzyaloshinskii−Moriya interactions that rotate along the chain as well as through a staggered g tensor.[15] These

interactions have also been used to explain unconventional spin gap behavior. In contrast to nonchiral systems, $[Cu(pym)(H_2O)_4]SiF_6 \cdot H_2O$ hosts a spin gap that is induced by and grows linearly with magnetic field.[15] The magnetization also increases linearly up to 50 T, at which point J becomes comparable to the Zeeman energy. The spins fully saturate near 70 T,[15] although the magnetization curves shown in the Supplementary Materials of Liu et al.[15] reveal several broad features between 50 and 70 T that depend on field orientation hinting at spin level crossings and/or magnetic ordering near the saturation field. μSR reveals a set of transitions near 3 and possibly 6 T that point toward possible magnetic ordering in applied magnetic field.[16]

In this work, we seek to understand the magnetic field - temperature (H - T) phase diagram of $[Cu(pym)(H_2O)_4]SiF_6 \cdot H_2O$ using electric polarization as a probe of certain symmetry breakings that signify long-range magnetic order. The study of
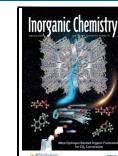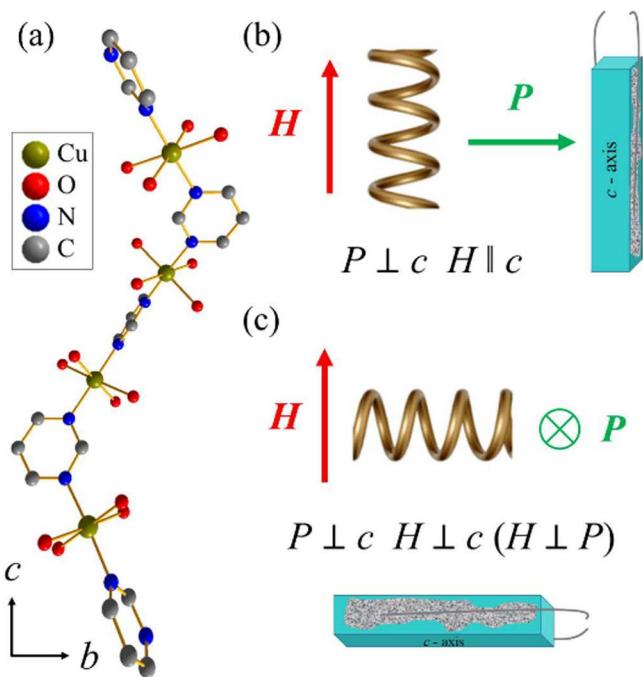
Figure 1. (a) Ball and stick representation of the chiral chain in $[Cu(pym)(H_2O)_4]SiF_6 \cdot H_2O$. Hydrogen atoms, uncoordinated water molecules, and SiF_6^{2-} anions are omitted for clarity. An extensive network of hydrogen bonds is formed between the chains through the uncoordinated water and silicon hexafluoride molecules. This system crystallizes in the $P4_12_12$ space group, so it is nonpolar, chiral, piezoelectric, and magnetic. Interestingly, it crystallizes in only left-handed helices. The Cu^{2+} centers are associated via a 4_1 screw symmetry. Note that the bond between the two nearest Cu^{2+} ions has no inversion center, which allows Dzyaloshinskii−Moriya interactions. The screw structure violates site-centered inversion symmetry as well. (b) Schematic of the $P \perp c$, $H \parallel c$ configuration of $[Cu(pym)(H_2O)_4]SiF_6 \cdot H_2O$. Here, H is the field (and magnetization) direction, the screw represents the chiral c-axis, and P is the polarization. (c) Diagram of the $P \perp c$, $H \perp c$ ($H \perp P$) measurement geometry.

high magnetic field phases via magnetization in copper coordination polymers is tricky because magnetization is difficult to measure cleanly in pulsed fields up to 75 T and is not necessarily sensitive to changes in a predominantly antiferromagnetic-like quantum state. We therefore turn to high magnetic field electric polarization, which is a symmetry-sensitive probe, in order to reveal the properties of this chiral spin chain. When magnetic field competes with a dominant J, the role of Dzyaloshinskii−Moriya and transverse coupling becomes increasingly important. There are several models in which a noncollinear spin configuration created by the Dzyaloshinskii-Moriya interaction becomes a mechanism for electric polarization.[17−23]

Electric polarization can be created via the displacement of charged ions or by orbital rearrangements as a lattice adjusts itself to slightly modify the Hamiltonian parameters and minimize the magnetic energy. The final lattice parameters and orbital configurations represent a balance between minimizing magnetic energy at the expense of lattice strain. These effects allow the magnetic order to alter the symmetry of the lattice and thereby create net electric dipoles. Thus, magnetic phase transitions and spin level crossings can be observed via magnetostriction[24] in most materials and also via electric polarization measurements for materials with appropriate

symmetries.[25] Notably, chiral materials have broken mirror planes and, by extension, broken spatial inversion symmetry. Broken spatial inversion symmetry is a necessary but not sufficient condition for the observation of electric polarization. The combination of broken spatial inversion and time-reversal symmetry at zero magnetic field can create linear magneto-electric coupling where an electric polarization is induced with magnetic field. On the other hand, a unique polar axis without rotational symmetry can support an electric polarization. $[Cu(pym)(H_2O)_4]SiF_6 \cdot H_2O$ does not satisfy either scenario required to host magnetoelectric coupling or electric polarization unless an additional magnetic symmetry-breaking occurs. Thus, the observation of either of these effects in applied magnetic field indicates a broken symmetry and likely magnetic ordering.

With these ideas in mind, we measured the change in electric polarization of the $S = 1/2$ chiral magnet $[Cu(pym)(H_2O)_4]SiF_6 \cdot H_2O$ as a function of magnetic field and used our results to develop a set of H - T phase diagrams that are quite different from what is observed in chemically similar linear chain systems like $Cu(pyz)(NO_3)_2$.[26−29] We find a striking series of phase transitions consistent with symmetry-breaking in combination with field-induced long-range magnetic ordering, magnetoelectric coupling, and striction effects. We discuss these results in terms of strong interchain coupling, Dyaloshinskii-Moriya interactions, and the ability of this system to stabilize noncollinear spin structures. Second-order magnetoelectric coupling in which the sign of the electric polarization is invariant under a change in magnetic field direction was observed. We employ these findings to suggest possible magnetic point groups for one of the field-induced magnetically ordered phases. Remarkably, some features in the H - T phase diagram survive to unexpectedly high temperatures. The primary high field phase boundary near 50 T also connects with a large capacitance peak near 134 K. In addition to hosting exotic phase diagrams with competing phases, chiral chains have the potential to deliver a wide range of unexpected properties including quenched magnetic order and spin liquid behavior - key ingredients for spintronics[30] and quantum information processing.[31]

■ METHODS

Single crystals of $[Cu(pym)(H_2O)_4]SiF_6 \cdot H_2O$ were grown using solution techniques as described previously.[14] Each crystal grows naturally as a single chiral domain and contains exclusively left-handed helices.[14] Pulsed high magnetic field electric polarization measurements were taken at the National High Magnetic Field Laboratory in Los Alamos, New Mexico using the capacitor-driven 65 T short pulse and 75 T duplex magnets. The single crystals were prepared by depositing parallel capacitance plates on opposing crystalline faces using silver paste, and leads were applied with platinum electrical wires to achieve desired configurations. To focus our efforts, we selected two of the five unique configurations for the majority of our measurements [Figure 1(b,c)]. Changes in polarization (ΔP) were measured as a function of pulsed magnetic field (H) by standard techniques.[32] These consist of recording the current between electrical ground and the capacitance plates as the magnetic field is changed using a Stanford Research 570 current to voltage converter. The electric polarization is the integral of the measured current, normalized to the surface area of the sample. Electric fields via voltages up to 100 kV/m can be applied before or during the measurements to samples. Switching the direction of the applied electric field while poling was able to switch the sign of ΔP in some configurations although the signal shape remained the same regardless of whichever poling protocol was employed. Being able to switch the
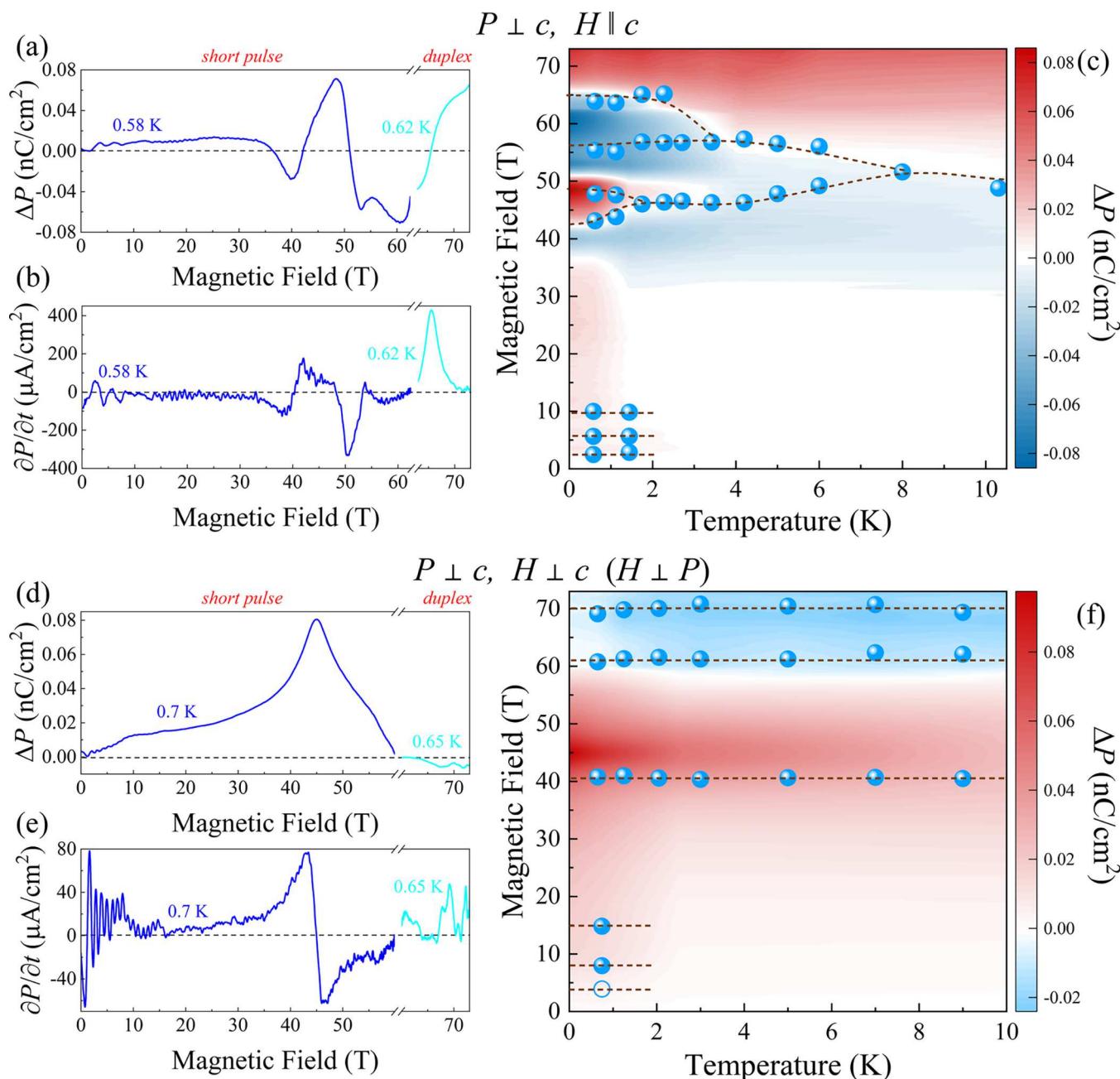
Figure 2. Magnetoelectric response of $[Cu(pym)(H_2O)_4]SiF_6\cdot H_2O$ in the $P \perp c$, $H \parallel c$ and $P \perp c$, $H \perp c$ ($H \perp P$) configurations. (a, d) Change in the electric polarization (ΔP) as a function of magnetic field for the $P \perp c$, $H \parallel c$ and $P \perp c$, $H \perp c$ ($H \perp P$) configurations, respectively. Data from the short pulse magnet is shown in navy blue, while data from the duplex magnet is shown in cyan. (b, e) Magnetoelectric current vs magnetic field in the indicated configurations. (c, f) H-T phase diagrams of $[Cu(pym)(H_2O)_4]SiF_6\cdot H_2O$ in two different configurations. The solid blue symbols indicate phase boundaries at various measurement temperatures. The open symbol represents a point with some uncertainty. Error bars are on the order of the symbol size, and the dashed lines guide the eye.

polarization direction by switching the electrical poling direction while keeping the magnetic field the same is a well-known phenomena and indicative of improper (magnetically induced) ferroelectricity.[33] To complement this work, we measured the infrared response of $Cu(pym)(H_2O)_4]SiF_6\cdot H_2O$ as a function of temperature and magnetic field.

■ RESULTS AND DISCUSSION

High Magnetic Field Polarization and Magnetic Field - Temperature Phase Diagrams. Figure 2(a) displays the change in electric polarization (ΔP) of $[Cu(pym)(H_2O)_4]$-$SiF_6\cdot H_2O$ with applied magnetic field in the $P \perp c$, $H \parallel c$

configuration. Here, we combine measurements on the short pulse 65 T magnet and the 75 T duplex magnet to overcome the 70 T saturation field.[15] At low magnetic fields, ΔP rises gradually, shows several small inflection points, reaches a plateau, and then changes sign near 36 T. It remains negative until 42 T, above which ΔP climbs to a maximum value of 0.072 nC/cm^2 at 49 T. ΔP goes negative again near 51 T and remains so to the limit of the short pulse magnet. From the duplex data, we see that ΔP switches sign one more time at 65 T and rises smoothly toward the 70 T critical field where there is only a slight change in slope to mark this important energy

scale. The magnetoelectric current, which is the derivative of ΔP, is shown in Figure 2(b). This quantity nicely highlights some of the smaller changes in polarization - for instance, those taking place below 12 T. By combining these data, we developed the magnetic field - temperature phase diagram.

Figure 2(c) displays the magnetic field - temperature phase diagram of $[Cu(pym)(H_2O)_4]$ $SiF_6 \cdot H_2O$ in the $P \perp c$, $H \parallel c$ configuration. Each of the blue data points is obtained from an analysis of the magnetoelectric current at a given temperature. We immediately notice the formation of clear phase boundaries that together map out several different areas in close proximity. The sign of the electric polarization change relative to zero magnetic field switches back and forth - from positive to negative - and back again several times. This behavior is especially dramatic below 2 K. Here, we find the three weak transitions at 3, 6, and 10 T that are probably due to magnetic field-induced spin rearrangements between magnetic orders that produce small overall positive electric polarization. These low field transitions are in good agreement with electron spin resonance and muon spin rotation data, which show transitions at similar fields.[15,16] The H - T phase diagram also displays a series a large swings in ΔP above 36 T, finally saturating above the 70 T critical field in a positive polarization phase. Increasing temperature brings some of these regions together, but even at 10 K, the sign of ΔP flips from negative to positive near 50 T. As we discuss below, this phase boundary survives to significantly higher temperatures.

Figure 2(d) displays the change in electric polarization with magnetic field in the $P \perp c$, $H \perp c$ ($H \perp P$) configuration. Once more, we make use of the 60 T short pulse and 75 T duplex magnets to cover the relevant field range. There is again a large magnetoelectric response but the sign of ΔP does not switch excessively as in the prior case. We find that ΔP increases steadily with magnetic field, revealing two or three weak features below 12 T and a maximum value of 0.081 nC/cm^2 near 40 T. Again, these low field phase boundaries are in good agreement with electron-spin resonance and muon-spin relaxation results indicating the presence of different magnetic field-induced magnetic states.[15,16] In Figure 2(d), ΔP drops sharply and goes negative at 60 T where it remains as the spins saturate. There is a small signature of the 70 T critical field (where the spin configuration saturates[15]). Figure 2(e) shows complementary magnetoelectric current data in the $P \perp c$, $H \perp c$ ($H \perp P$) configuration. Figure 2(f) displays the H - T phase diagram of $[Cu(pym)(H_2O)_4]SiF_6 \cdot H_2O$ in the $P \perp c$, $H \perp c$ ($H \perp P$) configuration. Overall, the phase diagram is beautifully simple with a maximum near 40 T and change in the sign of ΔP near 60 T.

Assigning the Various Phase Boundaries and Discussion of the Phase Diagrams. Further inspection reveals three main regions of the H - T phase diagrams of $[Cu(pym)(H_2O)_4]$ $SiF_6 \cdot H_2O$. We classify them as low, intermediate, and high magnetic field regions. In the low field regime, below 15 T, changes in the electric polarization are weak. Even so, we can identify three low temperature phase boundaries near approximately 3, 6, and 12 T. We assign these structures as field-induced transitions, consistent with electron-spin resonance and muon spin relaxation signatures in the vicinity.[15,16] Complementary magneto-infrared spectroscopy in this field regime is without contrast, ruling out a structural component to these features - at least at 4.2 K [Figure S5, Supporting Information]. This demonstrates that $[Cu(pym)-(H_2O)_4]SiF_6 \cdot H_2O$ behaves as a Type II multiferroic[34] with

electric polarization that is sensitive to different magnetic field-driven spin states. The intermediate magnetic field range is broad and featureless, separating the aforementioned magnetic transitions from the more exotic polarization changes at higher fields. The H - T phase diagram is very different in the high magnetic field region. Above 35 T, the magnitude of ΔP is significantly larger, and it switches signs in a dramatic fashion - at least in some configurations - from positive to negative and vice versa. Some, but not all, of these features dovetail with the magnetization.[15] For instance, magnetization in the $H \parallel c$ direction has a step near 55 T and saturates at 70 T.[15] This corresponds well with the two highest magnetic field phase boundaries in the $P \perp c$, $H \parallel c$ configuration [Figure 2(c)], although polarization displays other features as well. At the same time, magnetization in the $H \perp c$ configuration displays a small step near 60 T and saturation near 70 T.[15] Our phase diagram in the $P \perp c$, $H \perp c$ ($H \perp P$) configuration is in excellent agreement with these results. Surprisingly, the overall change in ΔP across the 70 T spin saturation transition is modest. The exact mechanisms behind these high magnetic field phases will, of course, be challenging to uncover as they are accessible only by pulsed magnetic field techniques at the present time. The short time scale of the magnetic field pulse obviously limits the types of measurements that are feasible.

The overall structure of the H - T phase diagrams summarized in Figure 2 and in the Supporting Information is dramatically different from what is encountered in quasi-one-dimensional Heisenberg antiferromagnets like Cu(pyz)-$(NO_3)_2$. This traditional linear chain magnet hosts a spin flop, magnetic field-induced spin canting, and a 14 T saturation field giving rise to a phase diagram with the simplest of structures and energy scales that are accessible even with a superconducting magnet.[26-29] Other quasi-one-dimensional antiferromagnets display similar magnetic field-driven transitions and states of matter.[35] By contrast, the H - T phase diagrams of $[Cu(pym)(H_2O)_4]SiF_6 \cdot H_2O$ host strong directional character with clear interchain interactions, extraordinary complexity, and overall larger energy scales - key differences that we attribute to the presence of structural chirality in this family of materials. Specifically, the chiral arrangement of Cu^{2+} ions, facilitated by meta-linked pyrimidine ligands, plays a crucial role in reducing the distance between $S = 1/2$ Cu^{2+} ions within the chain to 5.8 Å. Chirality also increases the near neighbor distance between magnetic ions in different chains to 7.431 Å. By way of comparison, Cu(pyz)$(NO_3)_2$ contains chemically similar molecular building blocks but no chirality because the Cu^{2+} centers are bridged by para-linked pyrazine ligands to yield nearly 180° bonding angles between magnetic ions. The distance between Cu^{2+} ions in the chain is 6.8 Å, and the interchain distance is 7.285 Å. These values are both longer and shorter than those in $[Cu(pym)(H_2O)_4]SiF_6 \cdot H_2O$, respectively.

These differences are reflected in the magnetic energy scales for this family of materials: Cu(pyz)$(NO_3)_2$ hosts $J = -10.6$ K and a 14 T magnetic saturation field[25,29] whereas $J = -42$ K and the saturation field is near 70 T in our system.[15] At the same time, Cu(pyz)$(NO_3)_2$ hosts an inter- to intrachain coupling ratio J'/J of $\sim 10^{-3}$ and orders antiferromagnetically at 105 mK. Our target compound does not order at zero magnetic field down to 20 mK.[15] It is possible that the interchain interactions could be frustrated in this system, thus creating quasi-one-dimensional behavior at zero field and long-range ordering at high fields.
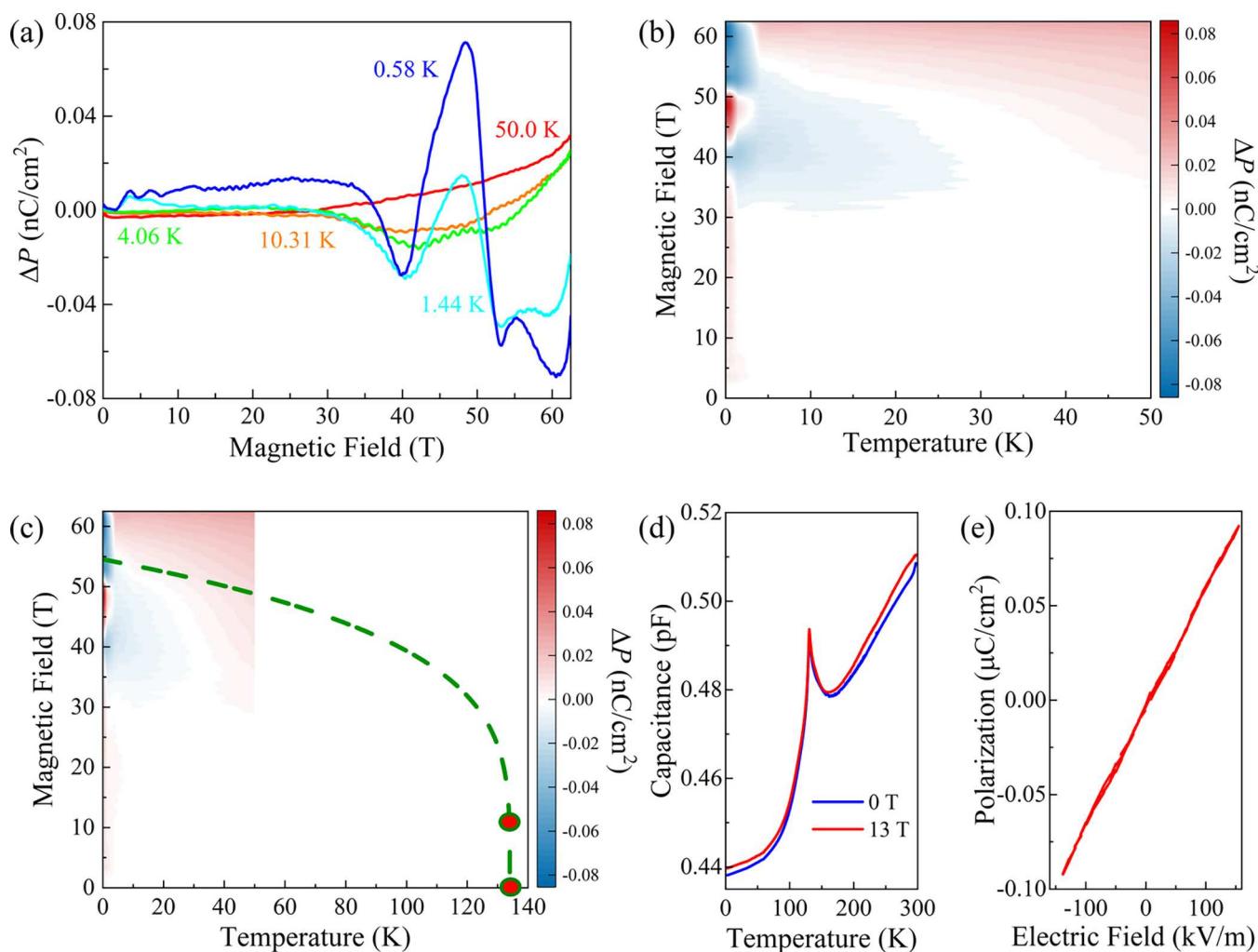
Figure 3. (a) Change in electric polarization (ΔP) as a function of magnetic field in the $P \perp c$, $H \parallel c$ configuration at several different temperatures. (b) Contour plot created by combining the electric polarization data over a wider temperature window including the 50 K data. (c) Contour plot of $[Cu(pym)(H_2O)_4]SiF_6 \cdot H_2O$ in the $P \perp c$, $H \parallel c$ configuration. This plot is the same data as panel (b) but with an extended temperature axis. The two points represent the capacitance peak positions, and the green dashed line is a power law fit of the highest phase boundary intersecting zero magnetic field at 134 K. (d) Capacitance measurements of $[Cu(pym)(H_2O)_4]SiF_6 \cdot H_2O$ in the $E \perp c$, $H \parallel c$ geometry at 0 and 13 T. The sharp peak at 134 K is present at both zero field and 13 T. (e) P - E loop of $[Cu(pym)(H_2O)_4]SiF_6 \cdot H_2O$ at 2 K.

High Temperature Behavior of the Chiral Spin Chain.
$[Cu(pym)(H_2O)_4]SiF_6 \cdot H_2O$ hosts interesting higher temperature effects as well. Figure 3(a) shows the change in electric polarization in the $P \perp c$, $H \parallel c$ configuration at different temperatures including 50 K, which was the highest temperature that we measured. Strikingly, ΔP is nonzero above 35 T, indicating that with strong enough magnetic fields, magneto-electric coupling can be observed near liquid nitrogen temperatures. Figure 3(b) displays the H - T phase diagram of the electric polarization in the $P \perp c$, $H \parallel c$ configuration incorporating the higher temperature data. Above 35 T the ΔP value is slightly positive and is indicated by a faint red color on the diagram. Figure 3(c) is identical to Figure 3(b), but with an extended temperature axis. The green dashed line is a power law fit showing where the principle high field phase boundary intersects the temperature axis at zero magnetic field.

Figure 3(d) displays the capacitance of $[Cu(pym)(H_2O)_4]$-$SiF_6 \cdot H_2O$ as a function of temperature. This measurement reveals a sharp peak at 134 K. Large capacitance peaks can be accompanied by structural distortions,[36,37] although in this case, X-ray diffraction demonstrates that the $P4_12_12$ space

group remains intact.[15] That said, careful examination of the crystallographic information files at 150 and 100 K reveals that some atom positions shift across this temperature range - particularly the hydrogen centers on coordinated and uncoordinated waters, resulting in subtle bond length and angle modifications. Infrared spectroscopy is consistent with this picture and provides clear evidence for enhanced low temperature hydrogen bonding but no structural transition [Figure S4, Supporting Information]. The essential point is that distortions involving hydrate ligands and free waters of crystallization do not alter the space group across 134 K [Figure 3(d)] - even though they do modify local structure. This feature does, however, provide an energy scale for possible gap opening. As shown in the extended H - T phase diagram of Figure 3(c), there is a reasonable power law fit correlation between high polarization field behavior and the energy scale of the capacitance peak both at 0 and 13 T. This shows that the 134 K transition temperature does hold some special electrical significance in our material. Figure 3(e) shows the P - E loop of $[Cu(pym)(H_2O)_4]SiF_6 \cdot H_2O$ at 2 K. The linear behavior is a sign of paraelectric character. The lack of

hysteresis shows that the material is not ferroelectric. We also measured the pyroelectric current from room temperature down to 2 K (not shown) and did not observe any pyroelectricity which indicates the material remains nonpolar down to very low temperatures in zero magnetic field consistent with the known space group of $P4_12_12$ and the lack of magnetic ordering at zero magnetic field.

Origins of Magnetoelectric Coupling. We have seen that $[Cu(pym)(H_2O)_4]SiF_6 \cdot H_2O$ displays field-induced magnetic ordering, and polarization switching, and second-order magnetoelectric coupling [Figure S3, Supporting Information]. In this section, we discuss possible magnetic point groups that can explain these behaviors and spin structures. The trends in the electric polarization are very complicated, preventing us from determining the magnetic point group of each phase. Therefore, we focus on the phase exhibiting the largest polarization. This phase resides between approximately 40 and 50 T. We note that there is probably no long-range magnetic ordering below 40 T, and above 70 T, the spin structure is simple with all spins aligned in the field direction.

In the free energy expansion, the linear magnetoelectric coupling term $\sum_{ij}\alpha_{ij}E_iH_j$ is followed by the second-order magnetoelectric coupling term ($\sum_{ijk}\beta_{ijk}E_iH_jH_k$). The indices i, j and k run from 1 to 3 and correspond to x, y and z. The former allows electric polarization to change sign with magnetic field whereas the latter is invariant under a change in magnetic field direction.

Second-order magnetoelectric coupling implies finite values for β_{111} or β_{222} (in-plane magnetic field inducing parallel in-plane electric polarization, Figure S2(a)), β_{122} or β_{211} (in-plane magnetic field inducing perpendicular in-plane electric polarization, Figure 2(d)), β_{311} or β_{322} (in-plane magnetic field inducing out-of-plane electric polarization, Figure S2(d)), β_{133} or β_{233} (out-of-plane magnetic field inducing in-plane electric polarization, Figure 2(a)), and β_{333} (out-of-plane magnetic field inducing out-of-plane electric polarization, Figure S2 (g)). We have scrutinized all 18 subgroups of 422.1' (magnetic point group 12.2.41), which is the paramagnetic magnetic point group of the title compound. Among these 18 subgroups, the magnetic point group 1.1' (magnetic point group 1.2.2)[38] symmetrically allows nonzero second order magnetoelectric coefficients consistent with our observations. It is of course possible that the spin structure induced by the magnetic field is so complicated that the magnetic point group becomes 1.2.2 while preserving the lattice symmetry.

Another possibility is that the magnetically ordered phase is not a subgroup of the parent magnetic point group 422.1'. For example, $m.1'$ (magnetic point group 4.2.10) with the following second order magnetoelectric coefficient matrix while the first order magnetoelectric coefficient is not allowed, can explain our observation:[38]

$$\beta_{ijk} = \begin{pmatrix} \beta_{111} & \beta_{122} & \beta_{133} & 0 & \beta_{113}(\beta_{131}) & 0 \\ 0 & 0 & 0 & \beta_{223}(\beta_{232}) & 0 & \beta_{212}(\beta_{221}) \\ \beta_{311} & \beta_{322} & \beta_{333} & 0 & \beta_{313}(\beta_{331}) & 0 \end{pmatrix} \quad (1)$$

Since $m.1'$ magnetic point group is not a subgroup of 422.1', stabilizing magnetic structure consistent with $m.1'$ requires an additional structural distortion. The title compound is a rather soft material compared with other conventional inorganic crystals with large empty space between chains and - as

explained previously - magnetic order may change the lattice configuration to minimize the total energy. As a consequence, our data is also consistent with this scenario. This means that we can not uniquely and inconclusively determine the magnetic point group of the ordered phase between 40 and 50 T.

That said, the parent crystallographic space group is not polar, and the observation of electric polarization under a magnetic field strongly indicates that the electric polarization has a magnetic origin. Several microscopic theories on the spin origin of electric polarization have been discussed.[39] Each theory requires a specific local symmetry condition; for example, the orbital hybridization model demands broken local inversion symmetry at the magnetic ions. Due to the structural chirality combined with a number of different atomic species surrounding the magnetic Cu^{2+} ions, the local symmetry of Cu^{2+} possesses the lowest symmetry. These conditions allow both local orbital hybridization between Cu^{2+} ions and ligands and a Dzyaloshinskii−Moriya interaction between Cu^{2+} ions.[15] Therefore, the asymmetric distribution of electron clouds near Cu^{2+} ions resulting from orbital hybridization and ligand displacements that accommodate Dzyaloshinskii−Moriya interactions should be considered seriously.[40−42] These factors could be responsible for a structural distortion, leading to a change in symmetry and contributing to the complex electric polarization behavior.

■ SUMMARY AND OUTLOOK

In order to explore field-induced transitions in a chiral $S = 1/2$ antiferromagnetic spin chain, we measured the electric polarization of $[Cu(pym)(H_2O)_4]SiF_6 \cdot H_2O$ as a function of magnetic field and compared our findings to expectations for quasi-one-dimensional analogs like $Cu(pyz)(NO_3)_2$ where canonical models for understanding many-body gaps and phase diagrams are well-established. We find a striking series of phase transitions consistent with symmetry-breaking in combination with long-range magnetic ordering, magneto-electric coupling, and striction effects. The H - T phase diagrams of the chiral magnet are dramatically different than those of the chemically similar linear chain system. We discuss these results in terms of strong interchain coupling combined with Dyaloshinskii-Moriya interactions, which act to stabilize noncollinear spin structures which, in turn, lower the symmetry of the system enough to produce novel polarization effects. These findings pave the way for the study of quantum magnetism in new settings and provide exciting opportunities to reveal new properties and states of matter under external stimuli that take advantage of the symmetry breaking that chirality delivers.

■ ASSOCIATED CONTENT

Ⓢ Supporting Information

The Supporting Information is available free of charge at https://pubs.acs.org/doi/10.1021/acs.inorgchem.4c01249.

Additional information on measurement configurations, pulsed field electric polarization results, and phase diagrams. The vibrational properties of $[Cu(pym)-(H_2O)_4]SiF_6 \cdot H_2O$ (PDF)

■ AUTHOR INFORMATION

Corresponding Author

Janice L. Musfeldt − *Department of Chemistry and Department of Physics and Astronomy, University of Tennessee, Knoxville, Tennessee 37996, United States*; Email: Musfeldt@utk.edu

Authors

Avery L. Blockmon − *Department of Chemistry, University of Tennessee, Knoxville, Tennessee 37996, United States*; orcid.org/0000-0002-0951-9832

Minseong Lee − *National High Magnetic Field Laboratory, Los Alamos National Laboratory, Los Alamos, New Mexico 87545, United States*

Shengzhi Zhang − *National High Magnetic Field Laboratory, Los Alamos National Laboratory, Los Alamos, New Mexico 87545, United States*

Zachary E. Manson − *Department of Chemistry, Biochemistry & Physics, Eastern Washington University, Cheney, Washington 99004, United States*

#Jamie L. Manson − *Department of Chemistry, Biochemistry & Physics, Eastern Washington University, Cheney, Washington 99004, United States*; orcid.org/0000-0003-2692-3500

Vivien S. Zapf − *National High Magnetic Field Laboratory, Los Alamos National Laboratory, Los Alamos, New Mexico 87545, United States*; orcid.org/0000-0002-8375-4515

Complete contact information is available at:
https://pubs.acs.org/10.1021/acs.inorgchem.4c01249

Author Contributions

$^{\perp}$A.L.B. and M.L. contributed equally to this work.

Notes

The authors declare no competing financial interest.
#Jamie L. Manson passed away in 2023.

■ REFERENCES

(1) Affleck, I. Quantum spin chains and the Haldane gap. *J. Phys.: Condens. Matter* **1989**, *1*, 3047.

(2) Chitra, R.; Giamarchi, T. Critical properties of gapped spin-chains and ladders in a magnetic field. *Phys. Rev. B* **1997**, *55*, 5816.

(3) Landee, C. P.; Turnbull, M. M. Recent Developments in Low-Dimensional Copper(II) Molecular Magnets. *Eur. J. Inorg. Chem.* **2013**, *2013*, 2266−2285.

(4) Zvyagin, S. Spin dynamics in quantum sine-gordon spin chains: high-field ESR studies. *Appl. Magn. Reson.* **2021**, *52*, 337−348.

(5) v. Löhneysen, H. v.; Beckmann, D.; Wosnitza, J.; Visser, D. Critical behavior of antiferromagnets with chiral symmetry. *J. Magn. Magn. Mater.* **1995**, *140-144*, 1469−1472.

(6) Kaburagi, M.; Kawamura, H.; Hikihara, T. Spin and chiral orderings of frustrated quantum spin chains. *J. Phys. Soc. Jpn.* **1999**, *68*, 3185−3188.

(7) Train, C.; Gruselle, M.; Verdaguer, M. The fruitful introduction of chirality and control of absolute configurations in molecular magnets. *Chem. Soc. Rev.* **2011**, *40*, 3297−3312.

(8) Naaman, R.; Paltiel, Y.; Waldeck, D. H. Chiral molecules and the electron spin. *Nature Reviews Chemistry* **2019**, *3*, 250−260.

(9) Yokouchi, T.; Kagawa, F.; Hirschberger, M.; Otani, Y.; Nagaosa, N.; Tokura, Y. Emergent electromagnetic induction in a helical-spin magnet. *Nature* **2020**, *586*, 232−236.

(10) Atzori, M.; Santanni, F.; Breslavetz, I.; Paillot, K.; Caneschi, A.; Rikken, G. L.; Sessoli, R.; Train, C. Magnetic anisotropy drives magnetochiral dichroism in a chiral molecular helix probed with visible light. *J. Am. Chem. Soc.* **2020**, *142*, 13908−13916.

(11) Lu, H.; Vardeny, Z. V.; Beard, M. C. Control of light, spin and charge with chiral metal halide semiconductors. *Nature Reviews Chemistry* **2022**, *6*, 470−485.

(12) Cheong, S.-W.; Xu, X. Magnetic chirality. *npj Quantum Materials* **2022**, *7*, 40.

(13) Yan, B. Structural chirality and electronic chirality in quantum materials. *Annu. Rev. Mater. Res.* **2024**, *54*, 10.1−10.9.

(14) Cordes, B.; David; Sharma, C. K.; Rogers, R. D. Enantiomorphic helical coordination polymers of {[M(pyrimidine)-$(OH_2)_4$][SiF_6]·H_2O}$_\infty$ (M = Co^{2+}, Cu^{2+}, Zn^{2+}). *Cryst. Growth Des.* **2007**, *7*, 1943−1945.

(15) Liu, J.; Kittaka, S.; Johnson, R.; Lancaster, T.; Singleton, J.; Sakakibara, T.; Kohama, Y.; Van Tol, J.; Ardavan, A.; Williams, B.; Blundell, S.; Manson, Z.; Manson, J.; Goddard, P. Unconventional field-induced spin gap in an S = 1/2 chiral staggered chain. *Phys. Rev. Lett.* **2019**, *122*, No. 057207.

(16) Lancaster, T. *Private communication*. 2023.

(17) Brockmann, M.; Klümper, A.; Ohanyan, V. Exact description of magnetoelectric effect in the spin-1/2 XXZ chain with Dzyaloshinskii-Moriya interaction. *Phys. Rev. B* **2013**, *87*, No. 054407.

(18) Thakur, P.; Durganandini, P. Factorization, coherence, and asymmetry in the Heisenberg spin-1/2 XXZ chain with Dzyaloshinskii-Moriya interaction in transverse magnetic field. *Phys. Rev. B* **2020**, *102*, No. 064409.

(19) Soltani, M.; Vahedi, J.; Abolhassani, M.; Masoudi, A. Heisenberg Model with Added Dzyaloshinskii-Moria Interaction. *International Scholarly Research Notices* **2011**, *2011*, 980192.

(20) Garate, I.; Affleck, I. Interplay between symmetric exchange anisotropy, uniform Dzyaloshinskii-Moriya interaction, and magnetic fields in the phase diagram of quantum magnets and superconductors. *Phys. Rev. B* **2010**, *81*, 144419.

(21) Thakur, P.; Durganandini, P. Heisenberg spin-1/2 XXZ chain in the presence of electric and magnetic fields. *Phys. Rev. B* **2018**, *97*, No. 064413.

(22) Chan, Y.-H.; Jin, W.; Jiang, H.-C.; Starykh, O. A. Ising order in a magnetized Heisenberg chain subject to a uniform Dzyaloshinskii-Moriya interaction. *Phys. Rev. B* **2017**, *96*, 214441.

(23) Guo, X.; Li, Y.; Yao, Z.; Jia, C.; Zhang, L. Spin chirality driven by the Dzyaloshinskii−Moriya interaction in one-dimensional antiferromagnetic chain. *AIP Advances* **2023**, *13*, No. 045103.

(24) Novoselova, I. P.; Petruhins, A.; Wiedwald, U.; Ingason, Á. S.; Hase, T.; Magnus, F.; Kapaklis, V.; Palisaitis, J.; Spasova, M.; Farle, M.; et al. Large uniaxial magnetostriction with sign inversion at the first order phase transition in the nanolaminated Mn_2GaC MAX phase. *Sci. Rep.* **2018**, *8*, 2637.

(25) Feng, D.; Zhu, Z.; Chen, X.; Qi, J. Electric-polarization-driven magnetic phase transition in a ferroelectric−ferromagnetic hetero-structure. *Appl. Phys. Lett.* **2021**, *118*, No. 062903.

(26) Hammar, P.; Stone, M.; Reich, D. H.; Broholm, C.; Gibson, P.; Turnbull, M.; Landee, C.; Oshikawa, M. Characterization of a quasi-

one-dimensional spin-1/2 magnet which is gapless and paramagnetic for $g\mu_B H \lesssim J$ and $k_B T \ll J$. *Phys. Rev. B* **1999**, *59*, 1008.

(27) Lancaster, T.; Blundell, S.; Brooks, M.; Baker, P.; Pratt, F.; Manson, J. L.; Landee, C.; Baines, C. Magnetic order in the quasi-one-dimensional spin-1/2 molecular chain compound copper pyrazine dinitrate. *Phys. Rev. B* **2006**, *73*, No. 020410.

(28) Günaydın-Şen, Ö.; Lee, C.; Tung, L.; Chen, P.; Turnbull, M.; Landee, C.; Wang, Y.; Whangbo, M.-H.; Musfeldt, J. Spin-lattice interactions through the quantum critical transition in Cu(pyz)-(NO$_3$)$_2$. *Phys. Rev. B* **2010**, *81*, 104307.

(29) Kono, Y.; Sakakibara, T.; Aoyama, C.; Hotta, C.; Turnbull, M.; Landee, C.; Takano, Y. Field-induced quantum criticality and universal temperature dependence of the magnetization of a spin-1/2 Heisenberg chain. *Phys. Rev. Lett.* **2015**, *114*, No. 037202.

(30) Yang, S.-H. Spintronics on chiral objects. *Appl. Phys. Lett.* **2020**, *116*, 120502.

(31) Lodahl, P.; Mahmoodian, S.; Stobbe, S.; Rauschenbeutel, A.; Schneeweiss, P.; Volz, J.; Pichler, H.; Zoller, P. Chiral quantum optics. *Nature* **2017**, *541*, 473−480.

(32) Zapf, V. S.; Kenzelmann, M.; Wolff-Fabris, F.; Balakirev, F.; Chen, Y. Magnetically induced electric polarization in an organometallic magnet. *Phys. Rev. B* **2010**, *82*, No. 060402.

(33) Israel, C.; Mathur, N.; Scott, J. A one-cent room-temperature magnetoelectric sensor. *Nat. Mater.* **2008**, *7*, 93−94.

(34) Khomskii, D. Classifying multiferroics: Mechanisms and effects. *Physics* **2009**, *2*, 20.

(35) Coldea, R.; Tennant, D.; Cowley, R.; McMorrow, D.; Dorner, B.; Tylczynski, Z. Quasi-1D $S = 1/2$ Antiferromagnet Cs$_2$CuCl$_4$ in a Magnetic Field. *Phys. Rev. Lett.* **1997**, *79*, 151.

(36) Hirose, N.; West, A. R. Impedance spectroscopy of undoped BaTiO$_3$ ceramics. *J. Am. Ceram. Soc.* **1996**, *79*, 1633−1641.

(37) Goossens, D. J.; Wu, X.; Prior, M. Structural phase transition in d-benzil characterised by capacitance measurements and neutron powder diffraction. *Solid State Commun.* **2005**, *136*, 543−545.

(38) Gallego, S. V.; Etxebarria, J.; Elcoro, L.; Tasci, E. S.; Perez-Mato, J. M. Automatic calculation of symmetry-adapted tensors in magnetic and non-magnetic materials: a new tool of the Bilbao Crystallographic Server. *Acta Crystallographica Section A: Foundations and Advances* **2019**, *75*, 438−447.

(39) Tokura, Y.; Seki, S.; Nagaosa, N. Multiferroics of spin origin. *Rep. Prog. Phys.* **2014**, *77*, No. 076501.

(40) Jia, C.; Onoda, S.; Nagaosa, N.; Han, J. H. Bond electronic polarization induced by spin. *Phys. Rev. B* **2006**, *74*, 224444.

(41) Jia, C.; Onoda, S.; Nagaosa, N.; Han, J. H. Microscopic theory of spin-polarization coupling in multiferroic transition metal oxides. *Phys. Rev. B* **2007**, *76*, 144424.

(42) Sergienko, I. A.; Dagotto, E. Role of the Dzyaloshinskii-Moriya interaction in multiferroic perovskites. *Phys. Rev. B* **2006**, *73*, No. 094434.